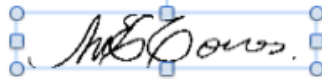# Oil & Natural Gas Technology

DOE Award No.: DE-FE0013531

Quarterly Research Performance
Progress Report (Period ending 3/31/2015)

Assessing the response of methane hydrates to environmental change at the Svalbard continental margin
Project Period (11/1/2013 to 10/31/2016)

Submitted by:
Marta E. Torres

Oregon State University
DUNS #: 053599908
104 COAS Admin. Bldg.
Corvallis, OR 97331-5503
e-mail: mtorres@coas.oregonstate.edu
Phone number: (541) 737-2902

Prepared for:
United States Department of Energy
National Energy Technology Laboratory

NETL

Office of Fossil Energy

EXECUTIVE SUMMARY

In November 2013, Oregon State University initiated the project entitled: **Assessing the response of methane hydrates to environmental change at the Svalbard continental margin**. In this project, we will take advantage of a unique opportunity to collect samples from the Svalbard continental margin. The overall objective of this research is to constrain the biogeochemical response of the gas hydrate system on the Svalbard margin to environmental change. The locations sampled shall provide key datasets that allow examination of the system with respect to sediment temperature fluctuations driven by thermal changes in the overlying water column and by hydrothermal circulation in the sediments. Because of a delay in the planned expedition, we reconfigured the program based on discussions with NETL program managers and submitted a revised SOPO. In the new plan, we will collect samples in two expeditions, the first of which happened Oct 7-21, 2014. However because of delays setting the project continuation going, we have not been able to make much progress the period from November 14 onwards. As we get the new revised contract in place, we can continue with the project

PROGRESS, RESULTS, AND DISCUSSION

1. Expedition(s) update: We have been invited to participate in the Norwegian led Expedition on the RV Helmer Hanssen to the Savalbard seep areas, which will take place May13-30, 2015. We began coordination of cruise objectives via a series of Skype meetings, followed with cruise preparations; protocol for sampling and analyses, ordering supplies, shipment to Norway etc.
2. Microbiology. Continued working on techniques for DNA extraction. In addition we secured a scholarship for graduate student Scott Klassek to perform incubation experiments this summer at the University of Shangai, China under the supervision of Prof. Fengping Wang. Samples collected during the RV H. Hanssen expedition will be shipped directly to China
3. Modeling- We continue to make progress in the computational models for methane hydrate formation at different methane fluxes. A draft of the paper is included. We expect this manuscript will be ready for submission this summer..

PROBLEMS OR DELAYS

No new problems since the set-back last year when the planned expedition in the R/V M.S. Merian got cancelled due to massive engine failure of the vessel. We continue to conduct expeditions to the area as documented in the revised project plan.

PRODUCTS

- Protocols for sampling during upcoming HH expedition
- Draft of computational model manuscript

RV Helmer Hanssen
May 2015 Expedition

Sampling protocols

Sampling procedure:

To be be prepared before coring
- Fill up 5ml 1M NaOH into 20ml glass serum vial, close it with stopper (no crimp)
- Label glass vials: content, analysis, date, cruise part,
- Production of 50ml 4% and 500ml 2% PFA buffer for cell fixation
- Agilent Vials containing 10μl $HgCl_2$
- Drill holes into the empty liner, cover holes with tape

CORING
1. Clean & label the core:
   large arrow pointing to the top of the core
   label core no. & cm (section no.) on each 30cm core intervals
   mark TOP & BOTTOM on each core section
2. Fill out the core log for the core
3. Cut core into 30-cm section
   4. Collect the sed. from the bottom end of the fresh cut core section
   5.
GAS ANALYSIS (every 30cm from bottom to top)

6. use 5-ml cut-off syringes
7. take the sed. through the pre-drilled hole in the liner- NO, this is from the fresh cut section of the core above
8. extrude 2 x 3ml sed. into 20-ml glass serum vial containing 5ml 1M NaOH
9. close with stopper and crimp-top
10. label with core no. & cm
11. store upside-down at 4C

RHIZONE SAMPLING (every 30cm from bottom to top)

12. Carry out the rhizone sampling within 4 hours of pulling up the cores (note hours)
13. Put Rhizone through the pre-drilled hole in the liner into the core sed.
14. Use *acid-washed* 20-mL syringes for shallower sediments (more water) and *acid-washed* 10-mL syringes for deeper sediments
15. Use woody sticks to keep vacuum in the syringes
16. Make a note of depth from the top of each core section (core no./section no.) for each rhizon sample

17. After porewater sampling leave Rhizones in the core sediment
18. Filter pore water through Accrudisk during subsampling

SO_4 precipitation test
19. add ~250μl porewater in clear PCR tube
20. add ~20μl $BaCl_2$
21. see if milky-white precipitate/turbidity forms → first sample where sulfate is abscent → SMTZ

POROSITY SAMPLING (every 30cm from bottom to top)

22. use 2-ml cut-off syringes
23. put **3ml sed**. into a *pre-weighed* **glass vial**
24. record exact volume taken
25. label with core no. & cm
26. store at ??? NOTHING SPECIAL, ROOM TEMPERATURE IS FINE

TOTAL SEDIMENT SAMPLING (BULK) (every 30cm from bottom to top)

27. take 1-2 scoops (~20ml) sed. via spoon or cut-off syringes
28. put into a Whirlpak bag
29. if calcium carbonate deposits are identified, take extra samples.

PORE WATER SUBSAMPLING

SALINITY TEST by Refractometer
30. Put a drop of porewater on the refractometer
31. record results
32. cleaned off between each sample using DI water and Kimwipes
33. calibrate refractometer periodically against sample of known salinity (IAPSO?)

$\delta^{13}C$
34. put 1ml pore water in an Agilent Vial containing 10µl $HgCl_2$
35. If H_2S is present, a brown precipitate will form

CHLORIDE
36. Put 2ml (min. 1ml) porewater in an empty Wheaton glass vial
SO_4
37. Add 1.5 ml porewater to a Wheaton glass vial OR 2-ml Eppendorf tubes) containing 0.1ml 10% ZnAc solution

NUTRIENTS
38. Put 3ml porewater in a 15-mL Falcon tube
39. Freeze at -20C

REMAINDER
40. Put remainder in acid-washed Nalgene bottles
41. Make sure bottles are tightly closed
42. put all Nalgene bottle samples from one core in a Ziploc freezer bag
43. Note how much porewater was added to each bottle
44. Acidify with ultra pure HNO_3^-

Microbiology program
Goals:
Analyze the samples to assess changes in chemistry and microbiology across vertical gradients (i.e., within a core) and horizontal gradients (i.e., across the putative upper edge of gas hydrate stability) that constrain the biogeochemical response at locations where methane hy-

drates are sensitive to environmental change. In particular, examine how microbial communities influence carbon, iron, manganese and sulfur cycling.

Samples for microbiological analysis will be obtained from the cores in close physical proximity to samples obtained for geochemical and physical parameters of the sediments.

DNA extraction samples should be put in liquid nitrogen as soon as possible. The RNA samples should also either be frozen in liquid nitrogen immediately or preserved with RNAlater to prevent RNA from breaking down. At the end of the expedition frozen samples will be shipped to OSU in dry shippers (MVE Biomedical Inc., Washington, PA) for analysis.

MICROBIOLOGY:
DNA/RNA (CAGE & OSU)
OSU: every 30cm within a 2-m range of the SMTZ
~1m (0.5m if SMTZ is shallow) above and ~1m below the SMTZ range
from the bottom of each core
4. use 50-ml cut-off syringes sterilized
5. extrude **50ml sed. into 50-ml Falcon tube** (2x)
6. label with core no. & cm
7. put tube into liquid N_2
8. store at -80C

NUMERICAL SIMULATION

MANUSCRIPT DRAFT

Methane hydrate formation in Ulleung Basin under conditions of variable salinity I. Reduced model and experiments

Wei-Li Hong _ Malgorzata Peszynska _
Marta Torres _ Ji-Hoon Kim

Methane hydrate formation in Ulleung Basin under conditions of variable salinity I. Reduced model and experiments

**Wei-Li Hong · Malgorzata Peszynska ·
Marta Torres · Ji-Hoon Kim**

Abstract Insert your abstract here. Include keywords, PACS and mathematical subject classification numbers as needed.

1 Introduction

This paper is the first of two in which we present an approximate or reduced model of methane hydrate evolution in subsea sediments under conditions of variable salinity. In this paper we describe the two-phase three-component physical model which is an simplification of comprehensive models in [19] and simultaneously a significant generalization of simpler models in [32]. Our model is rich enough to allow the study complex dynamics of hydrate formation under the conditions of variable salinity such as those in Ulleung Basin, and yet

W.-L. Hong
College of Earth, Ocean, and Atmospheric Sciences, Oregon State University, USA
E-mail: fauthor@example.com *Present address:* Center of Arctic Gas Hydrate, Environment, and Climate (CAGE), Arctic University of Norway

M. Peszynska
Department of Mathematics, Oregon State University, USA

M. Torres
College of Earth, Ocean, and Atmospheric Sciences, Oregon State University, USA

J.-H. Kim
Petroleum and Marine Research Division, Korea Institute of Geosciences and Mineral Resources, South Korea

is robust and fairly simple. In particular, we discuss in detail how the thermodynamics constraints are incorporated in the model and calibrated using experimental data. In the companion paper [**?**] we present details of numerical discretization with a particular emphasis on the variants of the time stepping, which are enabled by the approximations proposed here.

Gas hydrate is a frozen compound in which hydrocarbons are trapped in a water molecule lattice. Gas hydrates comprise a large and dynamic carbon reservoir; see [22, 9, 10]. In continental margin settings with high methane concentrations, gas hydrates occur naturally at water depths H greater than 300-500 mbsl (meters below see level), wherever enough methane is present. Numerous laboratory and field studies at gas hydrate bearing sites, including several drilling expeditions in the past decades, have provided critical background data on the conditions of gas hydrate stability, and have given an overall view of the composition and distribution of gas hydrates in nature (e.g. [30], and references therein).

Based on purely thermodynamic considerations, water and gas hydrate will co-exist in the sediment section that lies within the gas hydrate stability zone (HSZ or GHSZ). As temperature in the sediment increases according to the attendant geothermal gradient, a depth is reached where gas hydrate becomes unstable. Below this depth, water and free gas co-exist, but as long as there is water available in the formation, free gas should not be present within the HSZ. There is, however ample evidence of methane migration through the HSZ at gas-hydrate provinces worldwide. Observations of methane discharge at the seafloor, pressure core sampling imaging and analyses of methane concentrations at in situ pressures, acoustic blanking in seismic data, and logging data all support the vertical migration of gas through the HSZ, which in most cases result in formation of massive gas hydrate deposits at or near the seafloor.

The report of the presence of near-surface brines associated with massive gas hydrate deposits on Hydrate Ridge (Oregon), led to the development of hypotheses to explain this observation. Torres et al [32] used a one dimensional transient model to simulate the observed chloride enrichment and show that in order to reach the observed high chloride values, methane must be transported in the gas phase from the depth of the BSR to the seafloor. Methane transport exclusively in the dissolved phase is not enough to form methane hydrate at the rates needed to generate the observed chloride enrichment. As shown by [32], when enough free gas accumulates below the HSZ the excess (non-hydrostatic) pressure at the top of the gas layer may be sufficient to fracture the sediments and drive gas towards the seafloor. Alternatively, Liu and Fleming argue in [18] that as gas migrates from below the HSZ, gas hydrate formation depletes water, and elevates salinity enough to shift the until pore water local three-phase equilibrium to the point where liquid water, hydrate and free gas coexist, thus allowing vertical migration of free gas through the HSZ.

Since then, there have been additional observations of pore fluids highly enriched in dissolved chloride at sites of massive gas hydrate occurrence in northern Cascadia accretionary margin (Canada), the Krishna-Godavari Basin (India) and the Ulleung Basin (Korea). The sites drilled on seismic acoustic

chimneys indicative of free gas transport in the Ulleung Basin, all show chloride enrichments of up to 1440 mM from near-seafloor to depths of 100 meters below seafloor (mbsf). Below the depth of chloride maxima, however, chloride values approach concentrations that are lower or equal to seawater values, with minor negative chloride anomalies superimposed on baseline that reflect discrete gas hydrate bearing horizons [33]. None of these sites, however, show any evidence for the formation of a salinity front that can shift the thermodynamic equilibrium and sustain gas transport through the gas hydrate stability front, as postulated by current models [33].

In this paper we use the data from Ulleung Basin and compare these with the results of our new fairly simple model which includes the essential complexity encapsulated in the comprehensive models [19, 26]. In contrast to [32] and consistently with [19], our model implements equilibrium phase constraints known from thermodynamics [30, 7]. To test the applicability of our model we use the data from the 2010 UBGH2 expedition in which salinity spikes were observed close to the ocean floor. We use our model to hypothesize on what could have been the dynamics of hydrate formation that can explain these spikes. In contrast to [18] but in accordance with [33] we argue that large methane fluxes alone cannot explain these but rather that there must be a source of methane close to the observed anomalies. Our model assumes (i) hydrostatic and geothermal distributions of pressures and temperature, (ii) equilibrium phase transitions, (iii) incompressibility of fluids and porous medium. However it accounts for both transport modes: advective and diffusive, as well as for the two variables describing methane as well as salinity. It appears that (i) and (iii) are safe to assume for a large class of models, and that (ii) is natural given the time scales involved in the process.

The crux of our model rests on how the equilibrium phase behavior is implemented, and we follow our prior work [12, 25] in which the phase behavior is realized as an inequality constraint imposed on the methane solubility and implemented as a nonlinear complementarity constraint; we will refer to this construction as [NCC-M]. The [NCC-M] approach allows an easy construction of robust physically consistent models which approximate precise thermodynamics data, and can range from fully comprehensive models to simpler approximate time-stepping variants in which one or more variables are assumed known. In contrast, variable switching, a technique well known from multiphase multicomponent simulators, is formally equivalent to the fully implicit implementation of [NCC-M] for comprehensive models, but is not easily analyzed, specialized, approximated, or extended to non-implicit models. The advantage of our model over those in [19] is that each part can be carefully analyzed, tested, and validated, while such an endeavor is nearly impossible in more complex models in which the thermodynamics constraints use sparse look-up tables.

In this paper we describe in detail how our [NCC-M] model is calibrated. We use the software CSMGem [30, 1] to construct look-up tables for the approximate model. We compare these to several empirical and semi-empirical algebraic models in the literature. These comparisons show general consistency

but also differences between these approaches. The second paper [**?**] we provide crucial details of numerical discretization and discuss several variants of time-stepping which [NCC-M] approach enables.

The outline of the paper is as follows. We present the model in Sec. 2, and describe how it is calibrated using CSMGem and salinity data in Sec. 3. In Sec. 4 we describe the setup of simulations and in Sec. 5 compare their results to the experimental data from 2010 UBGH2 expedition. We close in Sec. 6 with conclusions. The Appendix provides details on some of the calculations and notation.

2 Reduced model of hydrate and salinity transport with methane hydrate formation

In the last decade roughly two classes of models for transport of gas hydrates were proposed. These are (i) fully comprehensive equilibrium models such as [19,11,6], and (ii) simpler conceptual models in [**?**,23,32], in which simplified kinetic or even simpler mechanisms for fluid equilibria were assumed. The model presented in this paper falls somewhere inbetween. It fits in the general framework of multiphase multicomponent models such as those in [17,**?**], uses bona-fide thermodynamics phase behavior models. and is in fact a direct simplification of the comprehensive model in [19]. The simplifications under which our model is constructed are reasonable for a wide class of simulations and case studies such as those of hydrate formation over thousands of years ([kyr]). The model we propose has enough complexity to describe coupled dynamics and transport of methane and salt components, yet is simple enough so that its various subsets are amenable to analyses and sensitivity studies. In particular, rigorous analysis of the diffusive transport model of methane was first discussed in [12], followed by a more general analysis in [25] of a model with advective/diffusive transport.

In this paper we describe the methane–salt model in a self-contained way which makes possible its use in real reservoir studies. In the companion paper [**?**] we present details of numerical solver for this model.

We consider transport of methane and salt in the sediment reservoir Ω under the ocean bottom; $\Omega \subset \mathbb{R}^d, d = 1, 2, 3$. Each point $x = (x_1, x_2, x_3) \in \Omega$ is at some depth $D(x)$ below the sea surface. In this paper we assume that x_3 points in the direction of gravity upwards and that the origin $x = 0$ is somewhere in, or beneath the reservoir. In 1D case $x = x_3$, and it is customary to consider a fixed reference depth $D_{ref} = H$ equal to the water depth H at seafloor, i.e., at the top of the reservoir. It is also convenient to consider the coordinate $z = D(x) - D_{ref} = D(x) - H$ measured in mbsf (meters below seafloor) which is used in other models [29]. In the general case of a 3D reservoir the bathymetry is variable, and $D(x)$ is measured relative to the sea surface rather than to the seafloor.

In this paper we are interested in the liquid and hydrate phases in Ω, thus we assume that the conditions in Ω are favorable for hydrate presence:

that is, that the pressure is high enough and temperature is low enough in Ω, and that there are sufficient sources of methane. The latter come from the advective gas fluxes reaching Ω from the direction of the Earth's center, or are provided by some methagenic sources [13]. The high pressure and low temperature conditions are possible at large depths H, or in Arctic regions. The properties of the sediment in Ω are its porosity ϕ_0 and permeability K_0, with $\phi_0 = \phi_0(x), K_0 = K_0(x)$; these are typically decreasing with overburden pressure, i.e., with $D(x)$. If hydrate is present, then the actual porosity $\phi(x)$ available to the liquid phase at x is $\phi = \phi_0 S_l$, where S_l is the liquid phase saturation, i.e., void fraction of the liquid phase. The actual permeability $K(x)$ in the presence of hydrate is an important property; however, it is not important in 1D case with constant flux.

In region Ω we have the following mass conservation equations for methane and salt components, respectively

$$\frac{\partial \phi_0 N_M}{\partial t} - \nabla \cdot D_M \nabla \chi_{lM} + \nabla \cdot (q \chi_{lM}) = f_M, \tag{1a}$$

$$\frac{\partial \phi_0 N_S}{\partial t} - \nabla \cdot D_S \nabla \chi_{lS} + \nabla \cdot (q \chi_{lS}) = 0. \tag{1b}$$

Here we have denoted by N_S, and N_M the (nondimensional) concentrations of methane and salt relative to water density, and by η_M, η_S their mass fractions, also called solubilities. The flux q is the volumetric Darcy flux of the liquid phase, and the diffusivities D_M, D_S are functions of S_l

$$D_C = D_C^0 \phi = D_C^0 \phi_0 S_l, \tag{1c}$$

where D_C^0 is the (molecular) diffusivity of the component C in bulk brine, and $\phi_0 S_l$ account for the decrease of solubility due to presence of porous medium [[17], *(2.2-20)*]. For components with (small) molecules of similar size, $D_C^0 \approx D^0 = 10^{-9} \mathrm{m}^2/\mathrm{s}$.

The mass conservation equations are complemented by the definitions

$$N_M = S_l \chi_M + R(1 - S_l), \tag{1d}$$

$$N_S = \chi_{lS} S_l. \tag{1e}$$

where R is a positive constant made precise below. Also, the source term f_M is given. The model is complemented by a pressure equation or some other relation defining q; see Sec. 7.2. In Sec. 2.1 we explain how the model is derived from first principles as a simplification of the comprehensive model from [19].

Assuming for the moment that q is known, we see that in (1) we have four equations and five unknowns: $N_M, N_S, \chi_{lS}, \chi_{lM}$ and S_l. After we eliminate N_M, N_S using (1d) and (1e), we have the two mass conservation equations (1a)-(1b) with three unknowns. The additional relationship which closes the system is the [NCC-M] phase constraint in which x, χ_{lS} are parameters

$$F(x, \chi_{lS}; \chi_{lM}, S_l) = 0, \tag{1f}$$

to be made precise in Section 2.2.

The model (1) must be supplemented with appropriate boundary and initial conditions, see Sec. **??**.

2.1 Details on (1)

The model (1) is a simplification of the first-principles comprehensive model in [19], see details in Sec. 7.1. We overview the simplifying assumptions here.

Denote by $P(x)$ and $T(x)$ the (liquid phase) pressure and temperature in the reservoir, respectively. Starting from seafloor, both $P(x)$ and $T(x)$ increase with depth [19] but may also be subject to some local variations due to, e.g., the seafloor temperature variations, or to the significant fluid fluxes against the hydrostatic equilibrium, or sediment heterogeneity. In this paper we assume that $T(x)$ is known and follows the geothermal gradient

$$T(x) = T_{ref} + (D(x) - D_{ref})G_T, \qquad (2a)$$

where T_{ref} is the temperature at some reference depth D_{ref} and $G_T \approx const$ is the geothermal gradient; see Section 4 for experimental values. The use of (2a) is common [7,?]; in [26] we showed little influence of a particular energy model for variable $T(x)$ on methane fluxes over long time period. See Sec. 4.2 for data.

The pressure $P(x)$ can be found from the pressure equation discussed in Section 7.2. However, the pressure is usually close to the hydrostatic $P_l^0(x)$ pressure

$$P(x) \approx P_l^0(x) := P_l^0|_{D_{ref}} + \rho_l G(D(x) - D_{ref}). \qquad (2b)$$

See Sec. 4.3 for data justifying (2b).

Next, the presence of the liquid and hydrate phase is accounted for by their saturations, i.e., void fractions, S_l, S_h, respectively. Since $S_l + S_h \equiv 1$, only one of these phase saturations is an independent variable. The two phases have respective densities ρ_l, ρ_h which are mildly dependent on the pressures and temperature. In our model we assume

$$\rho_l \approx const, \ \rho_h \approx const. \qquad (2c)$$

Similar incompressibility assumptions are commonly made in two-phase water-oil reservoir models [24,20], and (2c) is entirely reasonable over the time scale considered here.

The liquid phase consists of water, salt, and methane components, and their corresponding mass fractions in the liquid phase are denoted by $\chi_{lW}, \chi_{lS}, \chi_{lM}$, respectively. The hydrate phase is made of molecules of water and of methane, with the mass fractions denoted by χ_{hW}, χ_{hM}. Because of the physical nature of hydrate crystals built from a fixed proportion of methane and water molecules, it is common to assume the last two are constants, while $\chi_{lW}, \chi_{lS}, \chi_{lM}$ are variables. Since for mass fractions in the same phase we have $\chi_{lW} + \chi_{lS} + \chi_{lM} \equiv 1$ [[17], (2.2.8a)], therefore only two of the variables $\chi_{lW}, \chi_{lM}, \chi_{lS}$ can be independent, and in what follows we choose salt solubility χ_{lS} and one of methane related variables as the independent variables.

2.2 Solubility constraints

In this section we give details on (1f). The (maximum) amount of methane that can be dissolved in the liquid phase depends on the pressure P, temperature T, and the salinity χ_{lS}. Conversely, these variables determine the circumstances in which $S_l < 1$ and $S_h > 0$, i.e., when the hydrate phase can be present. From the hydrate literature [19, 30] it is known that *maximum solubility constraint* χ_{lM}^{max} depends on P, T, χ_{lS}

$$\chi_{lM}^{max} = \chi_{lM}^{max}(P, T, \chi_{lS}),$$

and there are tabulated data, or algebraic models, for χ_{lM}^{max}. There may be additional dependence of χ_{lM}^{max} on the type of sediment [6] but this will not be discussed here. Rather, we consider a particular approximation

$$\chi_{lM}^{max} \approx \chi_{lM}^{max}(x, \chi_{lS}) \approx \chi_{lM}^{max,0}(x) + \alpha(x)\chi_{lS}, \tag{2d}$$

consistent with models and data in literature. See Section 3 for details.

The quantity χ_{lM}^{max} determines how the total amount of methane N_M is partitioned between the liquid and hydrate phases. If $N_M(x,t) < \chi_{lM}^{max}$, then only the liquid phase is present, i.e., $S_l(x,t) = 1$, $N_M = \chi_{lM}$, and χ_{lM} is the independent variable which describes how much methane is dissolved in the liquid. On the other hand, when the amount present reaches the maximum amount that can be dissolved, i.e., $N_M \geq \chi_{lM}^{max}$, the excess of forms the hydrate phase with $S_h = 1 - S_l > 0$. In this case S_l becomes the independent variable while $\chi_{lM} = \chi_{lM}^{max}$ fixed.

These constraints [NCC-M] can be written concisely as a nonlinear complementarity constraint (NCC)

$$\begin{cases} \chi_{lM} \leq \chi_{lM}^{max}, & S_l = 1, \\ \chi_{lM} = \chi_{lM}^{max}, & S_l \leq 1, \\ (\chi_{lM}^{max} - \chi_{lM})(1 - S_l) & = 0. \end{cases} \tag{2e}$$

The companion paper [?] gives details on how (2e) is implemented in the different variants of time stepping applied in the numerical solver.

See Sec. 7.1 for details of how (1) is derived using (2).

2.3 Numerical model

The numerical model corresponding to (1) is based on a nonuniform structured grid in 1D, and 2D/3D. Discretization is cell-centered finite differences (FD) with harmonic averaging and mass lumping. We use operator splitting and treat advection explicitly and diffusion/equilibria implicitly, in several variants of time stepping applied to the coupled methane–salt system. The phase behavior (2d) is simplified and expressed with as $\chi_{lM}^{max}(x)$. For implicit parts we use Newton iteration, and [NCC-M] approach for the phase behavior.

Details are provided in the companion paper [?].

3 Model calibration

In order to apply the model (1) to realistic cases, we need data. In particular, we need data for χ_{lM}^{max}, also known as methane hydrate saturation (MHSAT), in (2e). In some models the estimates of MHSAT require the knowledge of methane hydrate stability pressure (MHEQ). In this section we compare various other theoretical and experimental approaches which provide MHSAT and MHEQ. This allows to understand the qualitative nature and sensitivity of this data, and provides the reader with various practical choices.

In comprehensive models such as [19] the data for MHSAT are provided via relatively sparse multivariate look-up tables involving several parameters such as pressure, temperature, and salinity. The sparsity of the data contributes to the roughness of the multivariate sampling, which in turn creates difficulties for a numerical solver, and as a result makes the results of the model critically dependent on the quality of the sampling. These difficulties can be exacerbated by the complexity of implementation of (1f), since this requires switching of Jacobian entries, and the use of numerical derivatives calculated from multivariate approximations, which can lead to further complications.

In our model we use the approximation (2d) supported by experimental data and/or theoretical thermodynamics analyses. This approximation provides clear dependence of MHSAT on the (few) primary unknowns of the model, thereby siplifying the phase behavior solver substantially. The approximation (2d) makes use of (2a), posisbly also of (2b), and of various known qualitative properties of MHSAT. In particular, it is known that the values of χ_{lM}^{max} in the hydrate stability zone HSZ are most strongly controlled by the temperature [29,7], with only a mild dependence on salinity, and with negligible dependence on the pressure, as long as MHSAT is sought within HSZ. By (2a) the temperature is a monotone function of depth, thus χ_{lM}^{max} is a function of depth $D(x)$ and of the salt mass fraction χ_{lS} as in (2d). In Sec. 3.3.1 we show how we construct a table for MHSAT in function of $D(x)$ and χ_{lS}.

As one of the approaches we consider the tabulated results of CSMGem. The code CSMGem was developed by Sloan and Koh [30,1] and calculates MEQ and MHSAT based on the statistical thermodynamics models proposed in [4,28,3]. CSMGem is an extension of CSMHYD which is publicly available [1]. Since this model is most detailed and up-to-date, we select it for our numerical simulations in Sec. 4. However, it is difficult to understand the qualitative nature of MHSAT or MHEQ from tabulated data alone, thus we provide comparisons with different models for MHSAT and MHEQ. In particular, we consider the model by Tishchenko et al. [31] which uses a semi-empirical approach based on the theoretical work from [27] to derive both MHEQ and MHSAT in conditions for $\chi_{lS} = 0$ (fresh water) to $\chi_{lS} = 2\chi_{lS}^{sw}$ (twice of seawater salinity). We also consider available experimental data.

In this paper we consider the stability and saturation of only structure I (sI) hydrate, with methane as the only guest component in the clathrate structure. Also, we consider NaCl as the only thermodynamic inhibitor. More generally, other electrolytes such as KCl or CaCl2 also serve as inhibitors (ref);

however, their effect is by an order of magnitude smaller than that of NaCl, and will be neglected.

First we discuss how we determine the HSZ where hydrate can coexist with liquid phase, and (1) is valid. Three phase equilibrium (aqueous-hydrate-vapor), i.e., MHEQ, are computed to find BHSZ, the depth of the bottom of HSZ. Above BHSZ we can consider only the two-phase aqueous-hydrate equilibria, and find MHSAT. We will assume that the values of $T(x), P(x), \chi_{lS}(x)$ are known at any $x \in \Omega$. The temperature $T(x)$ follows the geothermal gradient as in (2a), and the second either follows the hydrostatic gradient, or is known as a solution of the pressure equation (19) for some given boundary conditions. The third unknown, $\chi_{lS}(x)$ is actually an unknown of our model (1).

3.1 Calculation of MHEQ P_{eq}

The equilibrium pressure P_{eq} is the pressure at which the three phases: liquid, hydrate, and vapor, can coexist. In general, P_{eq} increases with the temperature T and decreases with the salinity χ_{lS}. Various estimates of the dependence of P_{eq} on T and χ_{lS} are shown in Fig. 1 including those from CSMGem, [21], and [31].

The model for $P_{eq}(T, \chi_{lS})$ from CSMGem that we use in simulations and shown in shown in Fig. 1 is obtained by running CSMGem for tabulated values of T, χ_{lS}. Alternatively, an algebraic model for P_{eq} is given in [21], where the lab measurements of MHEQ for variable salinity are fit with the following relationship

$$\ln(\frac{P_{eq}}{P_0}) = -926.815 + \frac{31979.3}{T} + 144.909 \ln(T)$$
$$+ 5847.92 \chi_{lS}^m + 322.026 (\chi_{lS}^m)^2 + 5840.5 \ln(1 - \chi_{lS}^m). \quad (3)$$

Here P_{eq} [MPa], T [K], and $P_0 = 0.101$ MPa is the atmospheric pressure, and χ_{lS}^m [mole/mole] is the mole fraction of NaCl in the aqueous phase; see Sec. 7.3. The relationship (3) is valid in conditions with salinity up to $\sim$8.5 times higher than seawater value and is in good agreement with laboratory data obtained under high salinity conditions [8,16].

As shown in Fig. 1, CSMGem values are close to those given by (3) and to a semi-empirical model from [31] for salinities $\chi_{lS} \leq \chi_{lS}^{sw}$, thus we can use (3) for qualitative discussions. However, for fluids with high salinity, the MHEQ estimated in [31] is greater than that estimated by CSMGem and the empirical relationship derived in [21].

3.2 Three phase equilibrium point(s) and the depth D_{eq} of BHSZ

From (3), and from $T = T(x)$ and $\chi_{lS} = \chi_{lS}(x,t)$ we see that $P_{eq} = P_{eq}(x,t)$. Recalling that the pressure $P = P(x)$, at a given x, t there may be (a) point(s)

Source	Model	P range [MPa]	T range [K]	S range [g/kg]
Experiments [21]	MHEQ	$P < 18$	$T < 290$	$[0, 20]$
Parametric approach [7]	MHSAT	$[10, 30]$	$[273, 300]$	$[0, S^{sw}]$
Semi-empirical approach [31]	MHEQ, MHSAT	$P < 50$	$[273, 297]$	$[0, 70]$
CSMGem [30]	MHEQ,MHSAT	?	?	

Table 1 Range of validity of MHEQ and MHSAT models in Section 3.3.1

$x = x_{eq}$ at some depth $D_{eq} = D(x_{eq})$ at which

$$x: \quad P(x) = P_{eq}(T(x), \chi_{lS}(x,t)). \tag{4}$$

The knowledge of D_{eq} and P_{eq} and $T_{eq} = T(x_{eq})$, is needed in the estimates of χ_{lM}^{max} as a function of x, and possibly of t.

Now x_{eq} is determined assuming that P, T, χ_{lS} are known. This is not true in general, and some useful approximations are reasonable in special cases.

First, assume hydrostatic pressure and constant salinity in 1D. In this case P, T are monotone in x and there is at most one such point x_{eq} with depth D_{eq} where (4) holds; this is the the base of HSZ. For depths $z < z_{eq}$ (or temperatures lower than T_{eq}), liquid in Ω can coexist with hydrate phase.

More generally, the salinity is nonconstant, and the conundrum is that we do not know $\chi_{lS}(x)$ when calculating D_{eq} from (4). Carrying this dependence forward is only possible in a complex comprehensive model, where a recalculation of MHEQ and MHSAT must be done at every point, and at every time step, and/or even within every iteration of the implicit solver. In the approximate model discussed in this paper we assume, as suggested in [7], that the salinity at the depths close to D_{eq} equals that of χ_{lS}^{sw}. This means that the base D_{eq} of HSZ is calculated once only, and is fixed. Therefore we identify BHSZ as the set of points x_{eq} for which

$$x_{eq}: \quad P(x_{eq}) = P_{eq}(T(x_{eq}), \chi_{lS}^{sw}). \tag{5a}$$

This approximation is clearly reasonable given the fact that it only determines BHSZ.

For variable salinity, nonhydrostatic pressure, or in more than one dimension, the depth of points x_{eq} needs not be unique, and it can vary in time. This has been taken into account in [18,19,6] but will not be considered here.

3.3 Model for MHSAT

Once we know D_{eq}, the values P_{eq} and T_{eq} are fixed. With these, one calculates the maximum solubility MHSAT, i.e., the maximum methane concentration at the three phase equilibrium, which is used in turn to get $\chi_{lM}^{max}(T(x), \chi_{lS}(x,t))$ at a given x, t.

We recall first the parametric model from [7] which provides a linear fit to data generated by the theoretical thermodynamics calculations from [34]; see also Tab. 1 in [7]. A reference point in this data provides a certain reference

pressure P_{ref}, and reference temperature T_{ref}, and solubility $C_3(T_{ref}, P_{ref})$ in pure water. A fit to the linear model

$$C_3(T, P) = C_3(T_{ref}, P_{ref})$$
$$+ \partial_T C_3(T_{ref}, P_{ref})(T - T_{ref}) + \partial_P C_3(T_{ref}, P_{ref})(P - P_{ref}), \quad (5b)$$

requires an estimate of $C_3(T_{ref}, P_{ref}), \partial_T C_3, \partial_P C_3$, see Tab. 2. **[MP correct/discuss the fit ? and comment]**. According to [7] $C_3(T, P)$ provides the solubility of methane (i.e., methane concentration) at the three phase equilibrium point. That is, at D_{eq} we obtain $C_3(T_{eq}, P_{eq})$ at the base of HSZ. To correct for the influence of salinity, and to find χ_{lM}^{max} at a given depth $D(x)$ within HSZ, in [7] it is proposed to use the model

$$C_{eq}(T(x), \chi_{lS}) = C_3(T_{eq}, P_{eq}) exp(\frac{T(x) - T_{eq}}{a})(1 - \beta \chi_{lS}^M), \quad (5c)$$

Here $a = 14.4K$, $\beta = 0.1mol^{-1}$ are the parameters determined from the theoretical calculation of Zatsepina and Buffett [34]Eq. (7). The variable χ_{lS}^M is the salinity in moles which has to be converted from $\chi_{lS}[kg/kg]$ **[WL: the unit of S in this equation is moles, see DavieZatsepinaBuffet2004 eq.7 ? Please check. I donot understand how S can be in moles]**. See also [29]Eq. (11), for (5c) calculated for pure water in heterogeneous sediments. Finally, we obtain χ_{lS}^{max} via the conversion factor

$$\chi_{lM}^{max}(x, \chi_{lS})[kg/kg] = C_{eq}(x, S)[mM]10^{-3}\frac{16.04}{1030}. \quad (5d)$$

Here we have used molecular weight of methane equal 16.04 g/mole, the seawater density 1030 g/L, and recalled that $1mM = 10^{-3}$ mole/L.

Combining (5d) with (5c) we see that the dependence of χ_{lM}^{max} on χ_{lS} is linear, as proposed in (2d). We calibrate our model (2d) to reflect this linear dependence in Sec. 4.

The model (5d) and various other parametizations and experiments of MH-SAT including CSMGem, [31,30,7,15], at three different pressure and five salinity values, are compared in Fig. 2. Estimates using fresh water and low pressure in [31] and [30] agree well with each other and with experimental results. As salinity increases, the estimates from both [31] and [7] suggest a reduction in MHSAT (i.e., the maximum methane concentration in equilibrium with hydrate decreases), in agreement with the laboratory results from [15]. CSMGem, however, suggests an increase in MHSAT as in Fig. 2, consistent with the theoretical calculation of [35], which also suggest an increase in MH-SAT at salinities higher than about 0.1 m. Finally, only few experimental data for high salinity are available [15], the evaluation of accuracy of theoretical analyses for high salinity is difficult. **[MP: comment on whether does the sign matters]**.

T_0	P_0	α	β	$C_3(T_0,P_0,S)$	$\partial_T C_3(T_0,P_0,0)$	$\partial_P C_3(T_0,P_0,0)$
292	20	14.4	0.1	153.36	6.34	1.11
K	MPa	oC	mol^{-1}	mM	mM/K	mM/MPa

Table 2 Parameters required in Equation (5b) to calculate methane hydrate stability and saturation following [7]. Recall that the unit of C_3 is mM and M (molarity) is mole/L.

3.3.1 Use of CSMGem to get χ_{lM}^{max}

In our numerical model we incorporate the MHEQ and MHSAT estimated by CSMGem. First, for a given $T(x)$ we calculate MHEQ. Then we use $P(x)$ to find the depth D_{eq} of BHSZ assuming seawater salinity at the depths close to the bottom of HSZ.

Next we use CSMGem to estimate MHSAT. We first construct a look-up table in which the input values of pressure P_i, temperature T_j, and salinity $\chi_{lS,k}$, cover the range of interest. For the pressures we consider the range between the seafloor pressure and that at the base of gas hydrate stability zone (BHSZ), Since pressure has relatively small effect on MHSAT, we only use these two values $P_1 = P_{ref}$ and $P_2 = P_{BSR}$ as the grid points. The temperature dependence is very significant, and we consider the interval $T_j \in [273K, 291K]$, with $\Delta T = 2$ K. We also consider salinity values $\chi_{lS,k} \in [0, 0.125]$kg/kg, where the right endpoint is four times the seawater salinity χ_{lS}^{sw}, with $\Delta \chi_{lS} = 0.0156$ for the total of nine grid points.

Next we use CSMGem to estimate MHSAT for each of the grid points $(P_i, T_j, \chi_{lS,k})$. This is done by trial and error: we provide CSMGem with some guess of χ_{lM}, and CSMGem predicts the phase conditions for $(P_i, T_j, \chi_{lS,k}, \chi_{lM})$. We try different values of χ_{lM} until we locate the MHSAT, the maximum methane concentration $\chi_{lM}^{max}|_{(P_i,T_j,\chi_{lS,k})}$ for which methane is only in two phases, i.e., as dissolved methane and methane hydrate. **[WL: I do not understand this sentence: The salinities are slightly different from the initial value we input as water volume change slightly due to hydrate formation.]** This process gives us a table of values

$$(P_i, T_j, \chi_{lS,k}, \chi_{lM}^{max}|_{(P_i,T_j,\chi_{lS,k})})$$

with $1 \le i \le 2, 1 \le j \le 20, 1 \le k \le 9$.

Next, for each grid point (P_i, T_j) we estimate the regression between the salinity $\chi_{lS,k}$ and MHSAT value $\chi_{lM}^{max}|_{(P_i,T_j,\chi_{lS,k})}$ over the range of salinity values $\chi_{lS,k}, k = 1, \ldots 9$. The regression provides us, for each (P_i, T_j) in the gridded table, with the coefficients A_{ij} and B_{ij} of the linear model so that

$$\chi_{lM}^{max}|_{(P_i,T_j,\chi_{lS,k})} = A_{ij} + B_{ij}\chi_{lS,k}.$$

As shown in Fig. 3, the values A_{ij}, B_{ij} are not very sensitive to the pressure, and it makes sense to approximate them using, e.g., $\bar{A}_j = A_{1j}, \bar{B}_j = B_{1j}$, corresponding to the top of reservoir, thus

$$\chi_{lM}^{max}|_{(P_i,T_j,\chi_{lS,k})} = \bar{A}_j + \bar{B}_j\chi_{lS,k}. \tag{6}$$

For cases where $P(x), x \in \Omega$ changes by more than 1-2 MPa, one may consider a more accurate multivariate model than (6).

In the last step we connect (6) to (2d). Based on (2a), each T_j corresponds to a unique depth D_j, thus we set-up a look-up table extending (6) to

$$\chi_{lM}^{max}(x,t) = \bar{A}(D(x)) + \bar{B}(D(x))\chi_{lS}(x,t) \tag{7}$$

where $\bar{A}(x), \bar{B}(x)$ are piecewise linear functions built from (D_j, A_j) and (D_j, B_j), respectively. Finally we identify that the form proposed in (2d) is (7) with $\chi_{lM}^{max,0}(x) := \bar{A}(D(x))$ and $\alpha(x) := \bar{B}(D(x))$. We also note that $\bar{A}$ and $\bar{B}$ correspond to the T-dependent and the χ_{lS}-dependent parts of (5c), respectively.

Finally we note that $\bar{B}$ found from tabulated data can have any sign. In fact, we find that it is positive, in contrast to the model (5c). **[MP comment]**

4 Application to the Ulleung Basin case

In this section we describe how the model (1) was calibrated using data from Ulleung Basin. The second drilling expedition to the Ulleung Basin (UBGH2) [2] offshore Korea (Fig. 4) drilled four sites that targeted the acoustic blanking chimneys in the seismic reflection data (Fig. 4(b)). These acoustic features extend from below the HSZ to near the seafloor, where they are usually accompanied by the presence of pockmarks or mounds on the seafloor bathymetry **[WL: REF ?]**. The seismic blanking zones have been interpreted to image conduits for gas migration, because of the low velocity of seismic waves as they travel through gas. Gas hydrates with different modes of occurrence were recovered from all four sites. From three of the sites (UBGH2-3, UBGH2-7, UBGH2-11), massive gas hydrates related to fracture filling (or grain displacing) morphology were observed at depths shallower than 6 mbsf [2],. Disseminated gas hydrates related to either fracture filling or pore filling modes were recovered from UBGH2-2_1 [2]. Finally, the porosity values were found to be

$$\phi_0 \in [0.6, 0.87], \tag{8}$$

with a few local anomalies down to 0.4.

4.1 Salinity data

Salinity, pressure and temperature conditions are fundamental in constraining the stability of gas hydrate. For the Ulleung Basin, the salinity data obtained shipboard is of less precision than dissolved chloride **[WL: REF]** we therefore use the chloride data and convert it to salinity (see Fig. 5) using the empirical relationship obtained by fitting all data from UBGH2 sites with
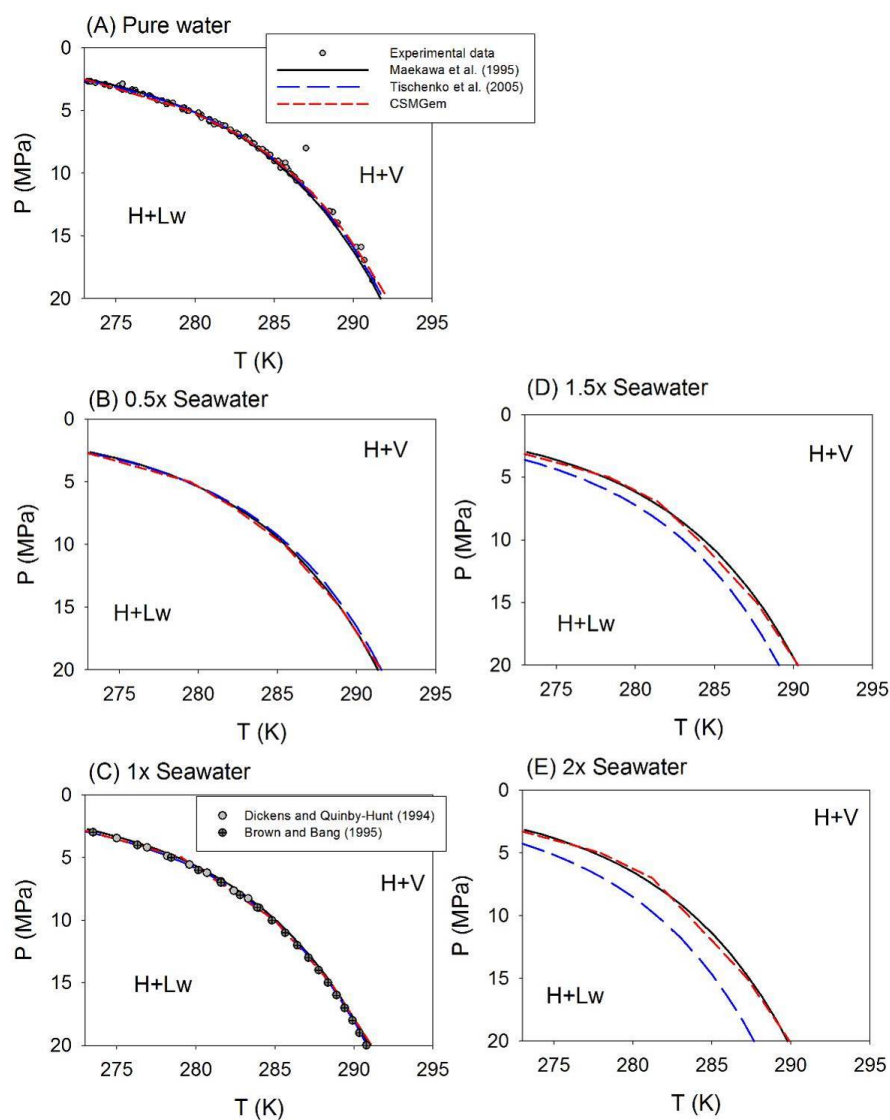
$$S_{ab} = 61.6Cl_M + 1.4301 \tag{9}$$

Fig. 1 Methane hydrate stability (MHEQ) for different salinity, pressure, and temperature estimated by various models. Available experimental data were shown for comparison. For salinity under seawater, all models agree well with each other and the experimental data. The stability field estimated by [31] strays away from the theoretical estimation by CSMGem and the estimation in [21] based on interpolation of experimental data.
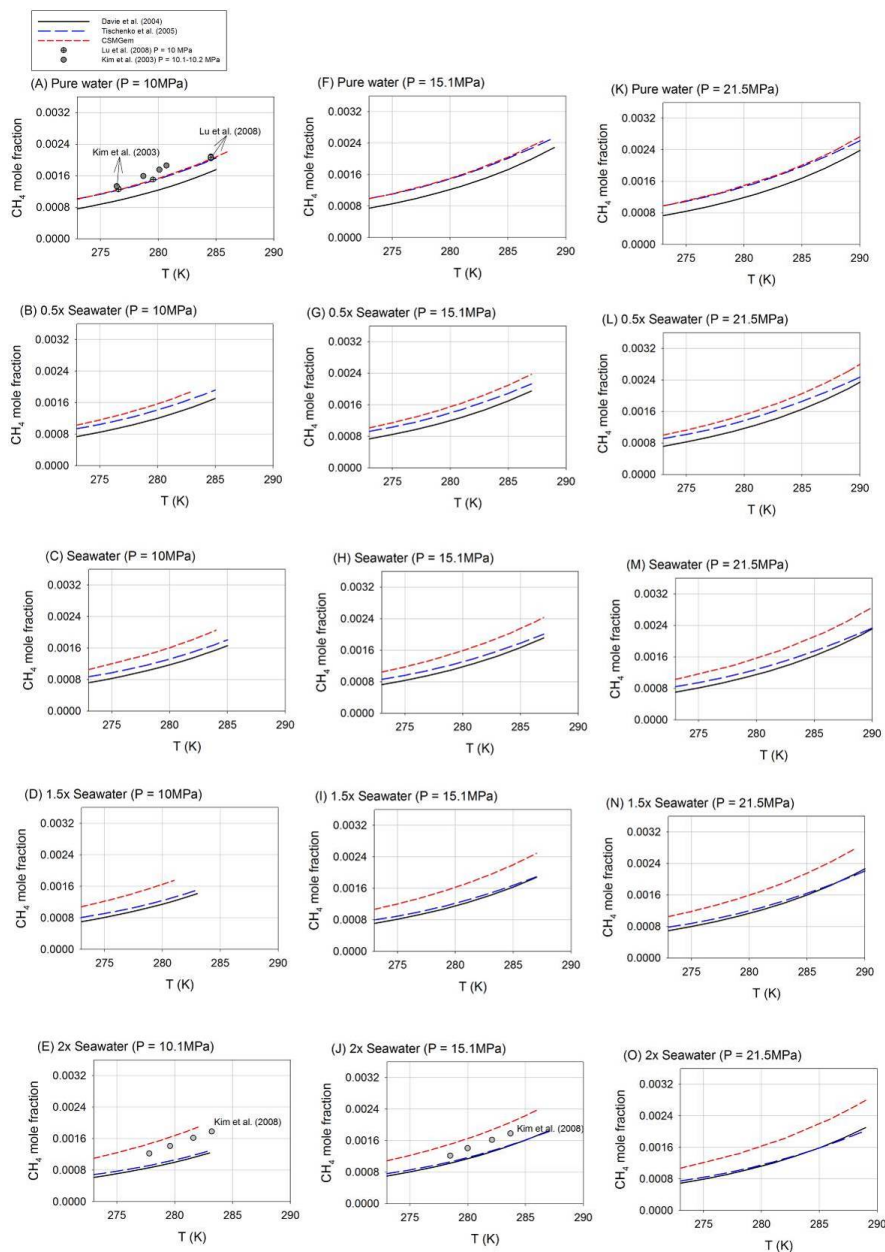
Fig. 2 Methane hydrate saturation (MHSAT) for different salinity, pressure, and temperature estimated by various models. Note that only few experimental data for pure water and $\chi_{lS} \approx 2\chi_{LS}^{sw}$ are available. The saturation estimated by CSMGem is always higher than the one estimated by [7] while the saturation estimated in [31] overlaps with one or the other approaches.
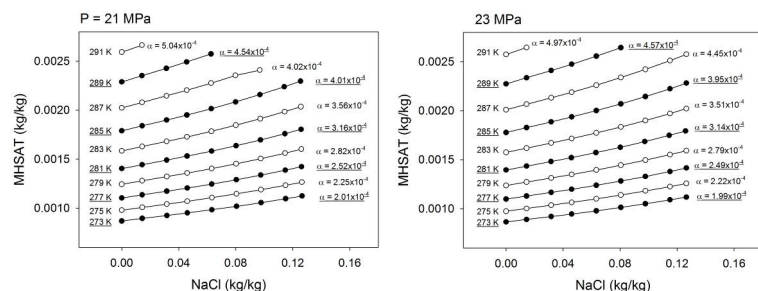
Fig. 3 The slope α between the salinity and MHSAT estimated from CSMGem as in (7). Positive value of α indicates that the methane hydrate is more difficult to form at higher salinity. Higher temperature elevates MHSAT and makes methane hydrate more difficult to form. MHSAT decreases only slightly when increasing pressure at the same temperature and salinity.

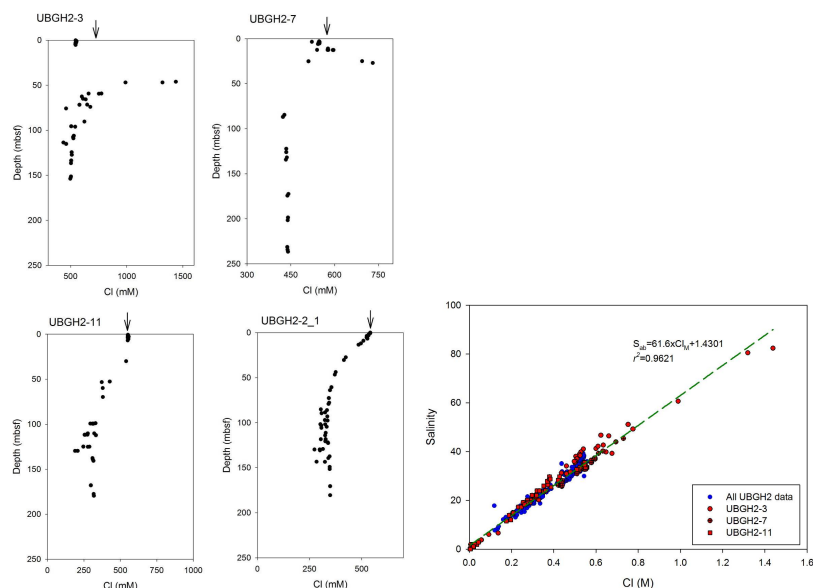**Fig. 4**   **[WL Figure 1: NEED Map]**

Fig. 5   Left: profiles of Cl in pore water for the four study sites. Right: empirical relationship between salinity and chlorinty for UBGH2 data.

[WL: why S_{ab} and not S ?] where Cl_M [M] is chlorinity. **[WL: is this necessary ? For comparison with the values reported in the literature, the salinity data is shown as a multiple of seawater salinity.]**

Pore water chloride profiles from these four sites reflect gas hydrate kinetics and fluid origins; see Fig. 5. Chloride concentrations at the bottom of the recovered sections are always lower than seawater, which have been interpreted as reflecting input of fresh water from clay mineral dehydration reactions at

depth [14]. The shallower sediment sections show different degrees of chloride enrichment at each site. At UBGH2-3 we have the most prominent chloride peak, with concentrations almost three times the seawater value. At UBGH2-11 and UBGH2-7, the enrichments range from a few millimolar to 180 M above seawater concentration, respectively. The site UBGH2-2_1 show the strongest signal of deep-sourced fresh water input, but has no enrichments in chloride. It is worth noticing that these enrichments in chloride concentration are minimum values, since they may be affected by gas hydrate dissociation during core recovery **[WL: REF).]**

4.2 Temperature data

The data from Ulleung Basin includes downhole temperature measurements as well as temperature T_{ref} at the seafloor. For other $T(x)$ we use (2a) where T_{ref} is seafloor temperature at depth D_{ref}, measured at each site, and G_T is local geothermal gradient, estimated by a fit of temperature profiles from downhole measurements to (2a), see Tab. 3.

4.3 Pressure and hydrostatic assumption

Further, we assume hydrostatic relationship (2b). The pressure at the seafloor, at the first gas hydrate appearance, and at the base of the HSZ are listed in Tab. 3. As shown, in a typical reservoir of thickness of 100 to 200 m, the pressure difference in the hydrostatic distribution is about $\Delta P_H \leq 2$ MPa, and it significantly exceeds the contrubutions to pressure difference that may occur due to advective fluxes.

Consider for example the range of depths $\Delta D(x)=100$ m. The hydrostatic pressure $P_l^0(x)$ gains $\Delta P_H = 1\text{MPa} \approx 9.8\text{m/s}^2 \cdot 10^3\text{kg/m}^3 \cdot 100\text{m}$ over ΔD, with the gradient $G_H \approx 10^6/100 = 10^4$ Pa/m. Now assume that the sediment has hydraulic conductivity around 1 cm/s, a high value corresponding, e.g., to gravel, and consistent with the porosity values (8) in Ulleung Basin. The conductivity 1 cm/s corresponds to the value K/μ in (19b) of around $10^{-6}\text{m}^2/\text{Pa} \cdot \text{s}$. Next assume advective flux $q = 0.1$ m/year $\approx 0.1/3.1510^{-7}$ m/s, a high value according to [5]. Calculate the corresponding $G = \Delta P/\Delta D = q/K$ which, after unit conversion, is less than 0.1 Pa/m, and appears insignificant compared to G_H. Pressure gradient G that would be comparable to G_H may occur only if the hydraulic conductiviy is several orders of magnitude lower, such as may occur in consolidated or clay sediments. Otherwise it makes sense to assume that pressure profile is essentially hydrostatic (2b).

	UBGH2-2_2	UBGH2-3	UBGH2-7	UBGH2-11
Seafloor depth $D_{ref} = H$[m]	2093	898	2145	2082
Pressure P_{ref} [MPa] at seafloor (a)	21.13	9.06	21.65	21.02
Temperature T_{ref} [K](b) at seafloor	273.35	273.45	273.55	274.35
BSR depth [mbsf]	180.5	131.6	124	159
P at BSR [MPa] (a)	22.95	10.39	22.90	22.62
BSR temperature [K] (c)	292.7	286	294.8	292.2
Salinity at BSR [kg/kg]	1.44E-2	2.94E-2	2.50E-2	1.73E-2
FGH depth [mbsf] (d)	67.9	6.2	7	7
P at FGH [MPa] (a)	21.81	9.13	21.71	21.09
FGH temperature [K](c)	273.4	274	274.6	275.1
Geothermal gradient G_T [K/m] (e)	0.107	0.095	0.171	0.120

Table 3 Basin parameters of the four study sites in Ulleung Basin. BSR is the bottom of HSZ **[WL: define BSR, check if =bottom of HSZ ?]**. FGH is the depth of first observed hydrate appearance. (a) Pressure was calculated assuming (2b). (b) Seafloor temperature was measured at each of the drilling site [?] **[WL: need ref to (Lee et al., 2013)]**. (c) Temperature is estimated from seafloor temperature and geothermal gradient with (2a). (d) The depth of hydrate first appearance was determined by visual observations of hydrate or by pore water anomalies. (e) Geothermal gradient G_T determined from linear regression of downhole temperature measurements at all UBGH2 drill-sites **[WL: need ref to (Riedel et al., 2013).]**

5 Model results and discussion

In this Section we apply our model to the case from UBGH2-7 case in Ulleung Basin in an effort to validate the model and to explain the coupled methane and salinity dynamics resulting in salinity spikes accompanying hydrate deposits. We use fully implicit numerical solver, with **[WL: please describe dx and dt you used]**.

The data from UBGH2-7 is along the vertical transsect and thus the case is essentially 1D, and we set up $\Omega = (0, L)$ where L is the reservoir thickness **[WL: is L=124 ? Your figures suggest over 200m]**. The bottom of the reservoir is at $x = 0$ and is above BHSZ **[WL: please check]**. We use T and P as described in Sec.4.2 and 4.3. We use relatively small advective flux q and thus, as discussed in Sec. 4.3, solving pressure equation is not necessary.

We set up the following boundary and initial conditions. The boundary conditions for methane and salt components are needed at $x = 0$ and $x = L$. For the top of reservoir $x = L$, i.e., sea bottom, we use seawater salinity and zero methane concentrations

$$\chi_{lM}(L,t) = 0, \quad \chi_{lS}(L,t) = \chi_{lS}^{sw}. \tag{10}$$

At $x = 0$, we assume conditions above BHSZ and set up boundary condition for methane to be given by MHSAT at the corresponding depth. For salinity at $x = 0$ we use the observed low salinity values χ_{LS}^0 **[WL: value ?]** shown in Fig. 5 following [14]

$$\chi_{lM}(0,t) = \chi_{lM}^{max}(0), \quad \chi_{lS}(0,t) = \chi_{lS}^0. \tag{11}$$

Case #	Diffusion rate D^0 (a) [m2/yr] (a)	Advection rate q [m/yr]	Peclet number	Methane source f_M (c) [kg/kg/kyr](c)	Time T [kyr]
1	$3 \cdot 10^{-2}$	$1.2 \cdot 10^{-9}$	$\ll 1$	0	25, 50, 100
2	$3 \cdot 10^{-2}$	$2 \cdot 10^{-4}$	1	0	25, 50, 100
3	$3 \cdot 10^{-2}$	$2 \cdot 10^{-2}$	166	0	2.5, 10, 25, 100
4	$3 \cdot 10^{-2}$	$1.2 \cdot 10^{-9}$	$\ll 1$	$8.3 \cdot 10^{-2}$	2.5, 5 10
5	$3 \cdot 10^{-2}$	$2 \cdot 10^{-3}$	16.6	$5 \cdot 10^{-2}$	10, 50, 100

Table 4 Parameters of the five simulation cases. (a) corresponds to the standard molecular diffusivity $10^{-9} \mathrm{m}^2/\mathrm{s}$. (b) 1 m/yr coresponds to $\approx 3 \cdot 10^{-5}$ mm/s. (c) kg of dissolved methane in 1 kg of seawater for every thousand years. Peclet number $Pe = qL/D$ where L is the characteristic length [WL: what did you use for L? how did you calculate Pe ?]

The initial conditions are

$$\chi_{lM}(x,0) = 0, \quad \chi_{lS}(x,0) = \chi_{lS}^0(x), \tag{12}$$

where $\chi_{lS}^0(x)$ is a linear function between $\chi_{LS}(0,t)$ and $\chi_{LS}(L,t)$.

We use reservoir parameters listed in Tab. 3 and set up five different scenarios to investigate how the profiles of dissolved methane concentration, salinity, and gas hydrate saturation respond to different modes of aqueous fluid transport. The cases are summarized in Tab. 4.

Cases 1, 2, and 3 compare simulation scenarios with different Peclet numbers as in Fig. 6-8. Advection transports the fluids with abundant methane from sources below HSZ, which facilitates the formation of hydrate, see Fig. 8. With a strong advective flux (Case 3), gas hydrate saturation reaches more than 30% after 100 kyr of simulation. This is in contrast to Cases 1 and 2 with Peclet numbers smaller or equal to 1.

However, even with very strong advection in Case 3, no brine is formed at any depth in the sediments. On the contrary, due to the strong fluid advection prescribed in this scenario, the whole sediment column is flushed with the fresh water. Such result contradicts the observations from our study sites, where shallow brine coexists with the abundant gas hydrate in the sediments in the upper 100 mbsf as in Fig. 5. A similar case study applied in [32] to Hydrate Ridge led the authors to conclude that the methane transport exclusively by advection is not sufficient to sustain the hydrate formation rate required to produce the observed salinity enrichment. A different source of methane other than aqueous transport from depth was postulated in [32] to be required.

In Case 4 we postulate therefore the existence of a source of methane $f_M \neq 0$ in the sediment section where abundant gas hydrate was observed (17 mbsf at UBGH2-7). In this simulation, we use minimum advective flux (Peclet number $\ll 1$ as in Tab. 4), and show that in response to the strong methane input, gas hydrate saturation exceeds the highest saturation obtained in Case 3 within 5 kyr. Because of the rapid formation of methane hydrate, dissolved ions accumulates in the pore fluids faster than are loss by diffusion to the overlying bottom water, leading to a brine patch above 50 mbsf. After running the model for 10 kyr, the hydrate saturation exceeds 60% and the salinity is

1.8 times higher than χ_{lS}^{sw} in bottom seawater, a value that is similar to what we observed in the pore water profiles in Fig. 9.

In Case 5 shown in Fig. 10 we include both large advective flux q and an arbitrary methane source $f_M \neq 0$. Similarly as in Case 4, gas hydrate saturation increases rapidly around the depths where methane source is present. However, the saturation is lower in Case 5 relative to that observed in Case 4 for the same model time (e.g., 10 kyr). This is because some of the methane is transported towards the seafloor by strong fluid advection. Besides, the methane hydrate in Case 5 spreads in a broader zone compared to observations in Case 4, because of the methane brought by advection from beneath HSZ. The magnitude of salinity enrichment is smaller than that in Case 4 because of dilution with the deep fresh fluid transported by the strong upward fluid advection.

We note that in Cases 4 and 5 one might argue that pressure equation should be solved to account for the local value of $\nabla \cdot q = f = f_M$ rather than (??) which suggests $\nabla \cdot q = 0$. However, the resulting pressure variations are not significant, even with f_M as assumed. A more general model should, however, account

5.1 Discussion

[WL, MT: please check this subsection]. The model (1) appears to reproduce the dynamics, and the hydrate and salinity profiles, in a manner consistent with the intuition. Furthermore, Case 4 gives results which are close to the profiles recorded in experiments. However, the presence of large source of methane f_M is needed to create the shallow brine patches, and the magnitude of f_M is not fully explained.

As shown in [13], methane production through organic matter degradation initiates at the depth where sulfate in the pore water is depleted and methane concentration starts to increase (i.e., [WL what is SMTZ ?]). Such depth may correspond to the location of the brine patches observed in Ulleung Basin. In Case 4 we tested therefore whether in situ methanogenesis could provide the methane required to sustain the rapid hydrate formation. Methanogenesis rates in Ulleung Basin, estimated from one chimney and one non-chimney site using a kinetic model constrained by pore water data, range from a few to 25 mmol/m3/yr [13]. Using the unit conversion (20) we see that the rate f_M assumed in Case 4 is significantly higher than the realistic rate of methanogenesis estimated in [13]. In other words, f_M proposed in [13] is not large enough to account simultaneously for rapid gas hydrate formation and the associated shallow brine observed in Ulleung Basin. Thus, while the simulation gives results consistent with the data, further hypotheses as to the nature of methane and salinity dynamics are needed. [WL, MT: do you agree with this statement].

Similarly to the reasoning used in [32] for the Hydrate Ridge case, we are led to conclude that the methane in the Ulleung Basin sites discussed here must be advecting in the gas phase from below the model domain. The
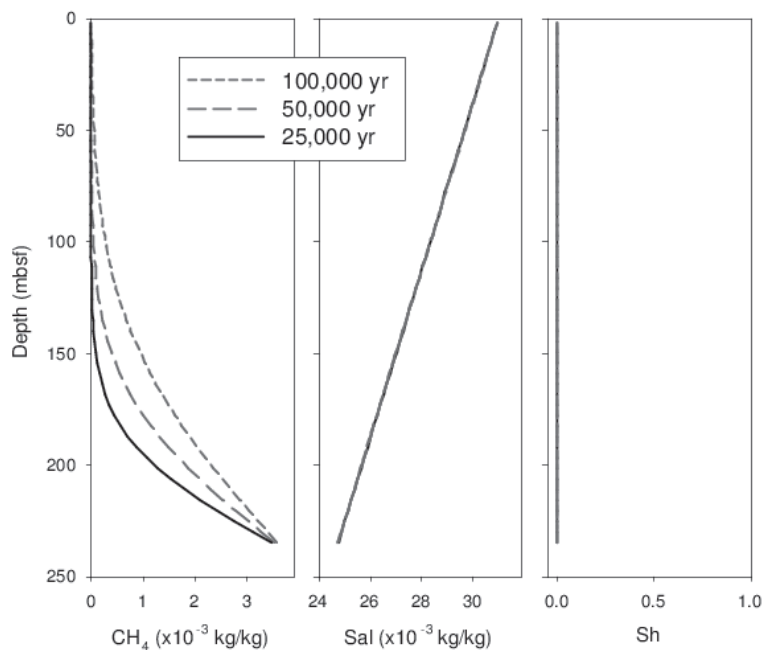
Fig. 6 Model results of Case 1.

methane solubility is too low for fluid advection to supply enough methane, with advection rate slow enough not to erase the positive salinity lense. Most likely, there is a source of gas below the HSZ, as imaged in seismic data, but free gas cannot travel through HSZ in the model (1) nor in comprehensive models [19] since these assume that water is abundant. Liu and Flemings in [18] hypothesized that the positive salinity anomaly that results from rapid hydrate formation at the base of the HSZ sustains a local three-phase equilibrium that allows methane gas to migrate upward and extends the saline tongue throughout the HSZ. Such extended positive salinity anomaly is, however, not observed in Ulleung Basin. Rather, the observed profiles as in Fig. 5 show that the brine is confined to shallow depths less than 50 mbsf, and to salinities lower than seawater salinities at depths greater than that.

6 Conclusions

In this paper we presented a reduced model of transport of methane and salt dissolved in liquid phase, with accompanying methane hydrate formation. The model was obtained from the comprehensive model such as [19] after several simplifiying assumptions were made; these assumptions are easily justified for basin modeling. The model is easily calibrated using phase behavior described
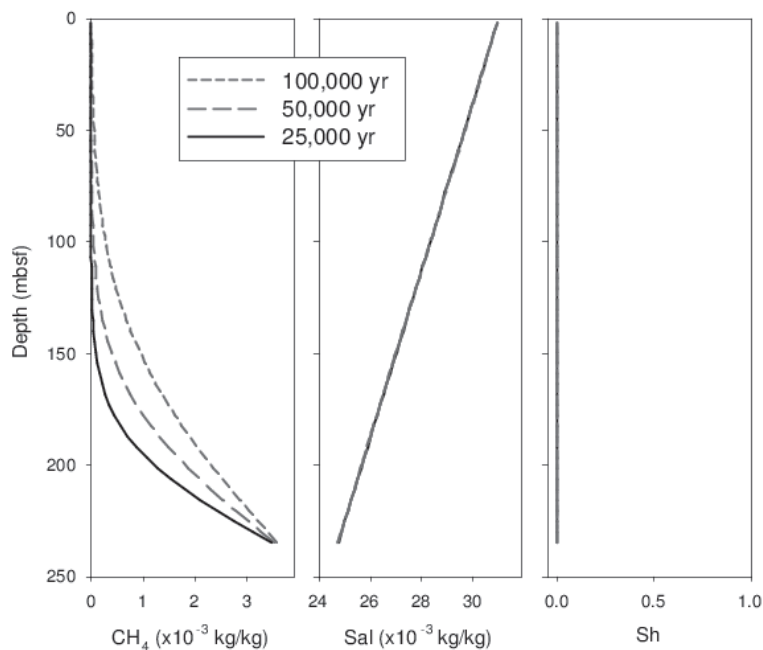
Fig. 7 Model results of Case 2.

in literature, and we described in detail good agreement between various empirical and algebraic models.

In addition, we were able to obtain good quantitative agreement between the model results and the data from Ulleung Basin based on postulated methanogenetic source. The results are consistent with previous work in [32] and [33]. On the other hand, the presence of fresh fluids in Ulleung Basin argue against development of a large positive salinity anomaly raising from the base of the HSZ to the seafloor as predicted by others, e.g., [18]. However, since such the methanogenetic source is not fully explained, there may be a separate mechanism needed for methane transport and presence of gas phase in HSZ in order to explain the salinity spikes which accompany hydrate patches.

7 Appendix

For completeness we recall here the notation as well as certain auxiliary conversion factors. We also provide details on modeling.
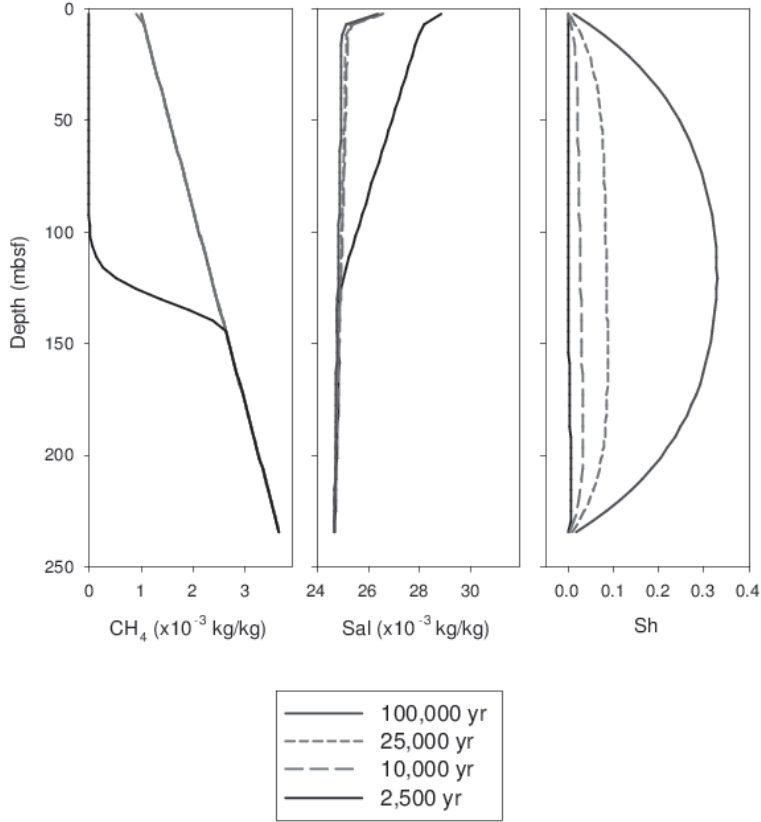
Fig. 8 Model results of Case 3.

7.1 Derivation of reduced model

The conservation of mass for the methane component in hydrate zone [19] takes the form

$$\frac{\partial}{\partial t}\left(\phi_0(S_l\rho_l\chi_{lM} + S_h\rho_h\chi_{hM})\right) + \nabla \cdot (q\rho_l\chi_{lM}) - \nabla \cdot (D_{lM}\rho_l\nabla\chi_{lM}) = \bar{f}_M \quad (13)$$

In this equation $\bar{f}_M$ is an external source of methane, e.g., due to bacteria–induced methanogenesis.

Now we assume (2c) The accumulation part (the term under the time derivative) can be rewritten with $N_M = \frac{\bar{N}_M}{\rho_l}$ as

$$N_M\rho_l = \bar{N}_M = S_l\rho_l\chi_{lM} + S_h\rho_h\chi_{hM} = S_l\chi_{lM} + (1-S_l)R.$$

where the (dimensionless) quantity R is

$$R := \frac{\rho_h\chi_{hM}}{\rho_l} \approx const, \quad (14)$$
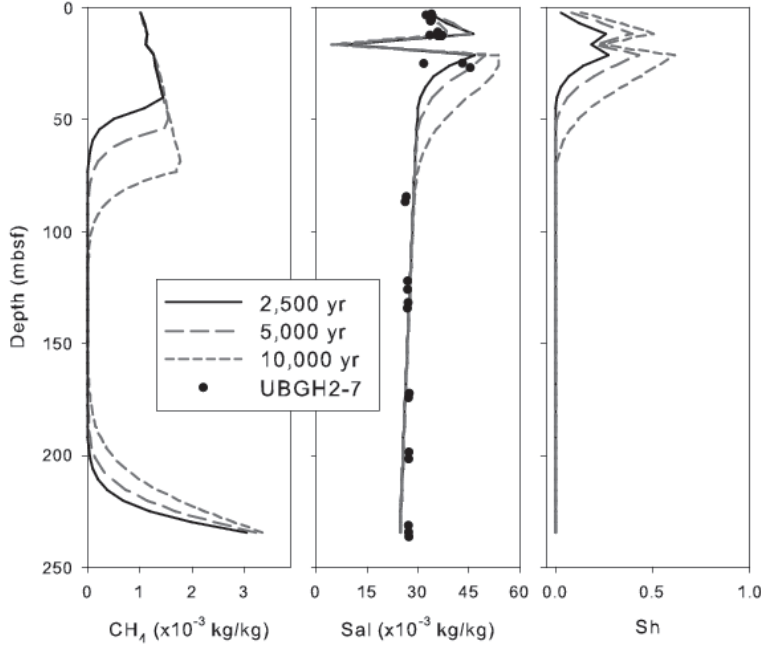
Fig. 9 Model results of Case 4. The observed salinity enrichment is matched to experimental data by adding an arbitrary source of methane.

Note that $\bar{N}_M$ is the total mass of methane per unit volume which accounts for the methane present both in the liquid and hydrate phases, and N_M is its dimensionless counterpart, relative to brine density.

Finally, it is useful to see that $S_l(x, t; N_M)$ is a function

$$S_l = \frac{N_M - R}{\chi_{lM} - R} = \begin{cases} 1, & N_M \leq \chi_{lM}^{max}(x, t), \\ \frac{N_M - R}{\chi_{lM}^{max}(x,t) - R}, & N_M > \chi_{lM}^{max}(x), \end{cases} \qquad (15)$$

Upon $f_M := \frac{\bar{f}_M}{\rho_l}$, and rescaling, we rewrite (13) in the form (1a).

Next, mass conservation for salt has the form

$$\frac{\partial}{\partial t}(\phi_0(S_l \rho_l \chi_{lS})) + \nabla \cdot (q \rho_l \chi_{lS}) - \nabla \cdot (D_{lS} \rho_l \nabla \chi_{lS}) = \bar{f}_S. \qquad (16)$$

and that for water

$$\frac{\partial}{\partial t}(\phi_0(S_l \rho_l \chi_{lW} + S_h \rho_h \chi_{hW})) + \nabla \cdot (q \rho_l \chi_{lW}) - \nabla \cdot (D_{lW} \rho_l \nabla \chi_{lW}) = \bar{f}_W \quad (17)$$

The structure of these equations is similar to that of (13) except that the salinity component is not present in the hydrate phase. Based on (2c) we can divide (16) by ρ_l; renaming $\chi_{lS} = \chi_{lS}$ we obtain the salinity part of (1).
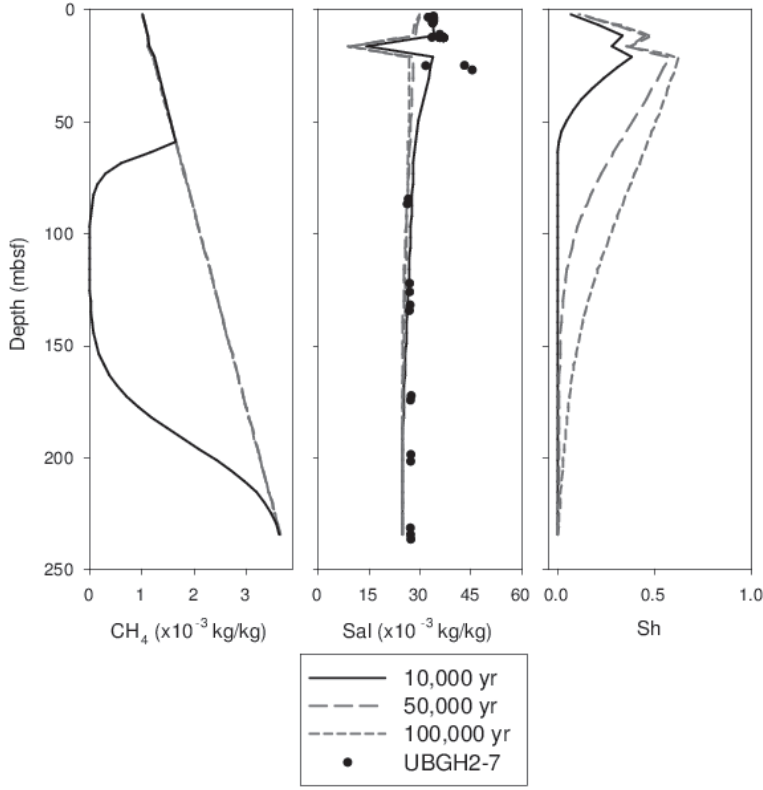
Fig. 10 Model results of Case 5.

7.2 Pressure equation

To derive the pressure equation, we add (13), (16), (17). Collecting terms and taking into account volume constraints $S_l + S_h = 1$ as well as $\chi_{lM} + \chi_{lS} + \chi_{lW} = 1$ and $\chi_{kM} + \chi_{hW} = 1$ we see that the accumulation term becomes $\frac{\partial}{\partial t}\phi_0(S_l\rho_l + S_h\rho_h)$. The advection term becomes $\nabla \cdot (q\rho_l)$, and the diffusion term

$$
\begin{aligned}
R_D &:= -\nabla \cdot (S_l\rho_l\phi_0(D_M^0\nabla\chi_{lM} + D_W^0\nabla\chi_{lW} + D_S^0\nabla\chi_{lS}) \\
&= -\nabla \cdot (S_l\rho_l\phi_0(D_M^0\nabla\chi_{lM} + D_W^0\nabla(1 - \chi_{lM} - \chi_{lS}) + D_S^0\nabla\chi_{lS}) \\
&= -\nabla \cdot (S_l\rho_l\phi_0((D_M^0 - D_W^0)\nabla\chi_{lM} + (D_S^0 - D_W^0)\nabla\chi_{lS}). \quad (18)
\end{aligned}
$$

Assuming that all diffusivities are equal, $\nabla \sum_{C=M,W,S} \chi_{lC} = \nabla(1) = 0$ and the diffusion term R_D vanishes. After further simplifications based on (2c) we obtain

$$
\frac{\partial}{\partial t}\left(\phi_0\big(S_l(1 - \frac{\rho_h}{\rho_l}) + \frac{\rho_h}{\rho_l}\big)\right) + \nabla \cdot q = f,
$$

Symbol	Definition	Units/ value
$x = (x_1, x_2, x_3)$	Spatial coordinate	[m]
ρ_l	Seawater density	1030 kg/m^3
g	Gravitational acceleration	9.8 m/s^2
$D(x)$	Depth of point x from sea level	[m]
$D_{ref}(x)$	Seafloor depth	[m]
	mbsl=meters below sea level	
	In 1D case $x = x_3$, $H = D_{ref}$	
$z = D(x_3) - H$	Depth below seafloor	[m]
	mbsf = meters below seafloor	
(G)HSZ	(Gas) Hydrate stability zone	
S_l	void fraction of liquid phase	
$S_h = 1 - S_l$	void fraction of hydrate phase	
χ_{lM}, χ_{lM}	mass fraction of methane in liquid phase	[kg/kg]
χ_{lS}, χ_{lS}	mass fraction of salt in liquid phase	[kg/kg]
$S = 10^{-3}\chi_{lS}$	salinity	[g/kg]
S^{sw}	seawater salinity	35 or 31 if only NaCl is present
T	Temperature	[K]
G_T	Geothermal gradient	[K/m]
ρ_h	Hydrate density	925 kg/m^3
χ_{pC}	Mass fraction of component C in phase p	kg/kg
χ_{hM}	Mass fraction of methane in hydrate phase	0.134 kg/kg
$R = \chi_{hM}\rho_h/\rho_l$	Constant used in defining methane concentration	0.1203 kg/kg
P	Pressure	[Pa,MPa]
G_H	Hydrostatic gradient	$\approx 10^4$Pa/m

Table 5 Notation and definitions used in the paper

where $f = f_M + f_S + f_W$. If furthermore ϕ_0 is assumed constant in time, and $\rho_h \approx \rho_l$, then, after some algebra, we obtain the steady state pressure equation

$$\nabla \cdot q = f. \tag{19a}$$

The equation (19a) is coupled with Darcy's law

$$q = -\frac{K}{\mu}(\nabla P_l - \rho_l G \nabla D(x)) \tag{19b}$$

In the absence of sources and $f \equiv 0$, q is divergence free. In the 1D case, $q = const$ and is equal to the flux across the boundary $\partial\Omega$. In fact, the pressure is usually close to the hydrostatic $P_l^0(x)$ pressure defined by (2b).

7.3 Conversion factors

[WL: please check. I changed your conversion factors because I do not think they were correct ?] The conversion factor between χ_{lS} and χ_{lS}^m is computed as follows. Assume we have $1L$ seawater with weight 1.03kg= 1030g. Let the salinity be $\chi_{lS} = 0.035$kg/kg. In the volume of 1L this

corresponds to $0.035 * 1030 = 36.05$g. Using molecular mass of 58.44g/mole of NaCl, we see that this gives $36.05/58.44 = 0.62$ moles of NaCl. The same volume 1L of sewater has $N = 1030/18.02 = 57.2$ moles, since 18.02g/mole is the molecular weight of water. Thus the mole fraction corresponding to $\chi_{lS} = 0.035$ and $S = 35$ is therefore $\chi_{lS}^m = 0.62/(0.62 + 57.2) = 0.01$.

Further conversion factors are needed. In particular, for f_M, we have

$$1\frac{mmol}{m^3 yr}$$
$$= 10^{-3}\frac{mol}{m^3 yr} \times 16\frac{g}{mol} \times 10^{-3}\frac{kg(CH_4)}{g} \times \frac{1}{1030}\frac{m^3}{kg(SW)} \times 1000\frac{yr}{kyr}$$
$$= 1.55 \times 10^{-5}\frac{kg(CH_4)}{kg(SW)kyr} \quad (20)$$

References

1. Center for Hydrate Research Software CSMHYD and CSMGem. URL http://hydrates.mines.edu/CHR/Software.html. Accessed April 9, 2015
2. Bahk, J., Kim, G.Y.: Characterization of gas hydrate reservoirs in the Ulleung Basin, East Sea (Korea), by integration of core and log data. Marine and Petroleum Geology **47**, 30–42 (2013)
3. Ballard, A.L.: A non-ideal hydrate solid solution model for a multi-phase equilibria program (2002)
4. Barrer, R., Stuart, W.: Non-stoichiometric clathrate compounds of water (1957)
5. Berndt, C., Feseker, T., Treude, T., Krastel, S., Liebetrau, V., Niemann, H., Bertics, V.J., Dumke, I., Dunnbier, K., Ferre, B., et al.: Temporal constraints on hydrate-controlled methane seepage off Svalbard. Science **343**(6168), 284–287 (2014)
6. Daigle, H., Dugan, B.: Capillary controls on methane hydrate distribution and fracturing in advective systems. Geochemistry, Geophysics, Geosystems **12**(1) (2011)
7. Davie, M., Zatsepina, O.Y., Buffett, B.: Methane solubility in marine hydrate environments. Marine Geology **203**(1), 177–184 (2004). DOI 10.1016/s0025-3227(03)00331-1
8. De Roo, J., Peters, C., Lichtenthaler, R., Diepen, G.: Occurrence of methane hydrate in saturated and unsaturated solutions of sodium chloride and water in dependence of temperature and pressure. AIChE Journal **29**(4), 651–657 (1983)
9. Dickens, G.R.: (2001)
10. Dickens, G.R.: Rethinking the global carbon cycle with a large, dynamic and microbially mediated gas hydrate capacitor. Earth Planet. Sci. Lett. **213** (2003)
11. Garg, S., Pritchett, J., Katoh, A., Baba, K., Fijii, T.: A mathematical model for the formation and dossociation of methane hydrates in the marine environment. Journal of Geophysical Research **113**, B08,201 (2008)
12. Gibson, N.L., Medina, F.P., Peszynska, M., Showalter, R.E.: Evolution of phase transitions in methane hydrate. Journal of Mathematical Analysis and Applications **409**(2), 816 – 833 (2014). DOI http://dx.doi.org/10.1016/j.jmaa.2013.07.023. URL http://www.sciencedirect.com/science/article/pii/S0022247X13006628
13. Hong, W.L., Torres, M.E., Kim, J.H., Choi, J., Bahk, J.J.: Towards quantifying the reaction network around the sulfate–methane-transition-zone in the Ulleung Basin, East Sea, with a kinetic modeling approach. Geochimica et Cosmochimica Acta **140**, 127–141 (2014). DOI http://dx.doi.org/10.1016/j.gca.2014.05.032
14. Kim, J.H., Torres, M.E., Hong, W.L., Choi, J., Riedel, M., Bahk, J.J., Kim, S.H.: Pore fluid chemistry from the Second Gas Hydrate Drilling Expedition in the Ulleung Basin (UBGH2): Source, mechanisms and consequences of fluid freshening in the central part of the Ulleung Basin, East Sea. Marine and Petroleum Geology **47**, 99–112 (2013). DOI 10.1016/j.marpetgeo.2012.12.011

15. Kim, Y., Lim, B., Lee, J., Lee, C.: Solubilities of carbon dioxide, methane, and ethane in sodium chloride solution containing gas hydrate. Journal of Chemical & Engineering Data **53**(6), 1351–1354 (2008)

16. Kobayashi, R., Withrow, H., Williams, G., Katz, D.: Gas hydrate formation with brine and ethanol solutions. In: Proceeding of the 30th Annual Convention, Natural Gasoline Association of America, pp. 27–31 (1951)

17. Lake, L.W.: Enhanced oil recovery. Prentice Hall (1989)

18. Liu, X., Flemings, P.B.: Passing gas through the hydrate stability zone at southern hydrate ridge, offshore oregon. Earth and Planetary Science Letters **241**(1), 211–226 (2006)

19. Liu, X., Flemings, P.B.: Dynamic multiphase flow model of hydrate formation in marine sediments. Journal of Geophysical Research **112**, B03,101 (2008)

20. Lu, Q., Peszyńska, M., Wheeler, M.F.: A parallel multi-block black-oil model in multi-model implementation. SPE Journal **7**(3), 278–287 (2002). SPE 79535

21. Maekawa, T., Itoh, S., Sakata, S., Igari, S.i., Imai, N.: Pressure and temperature conditions for methane hydrate dissociation in sodium chloride solutions. GEOCHEMICAL JOURNAL-JAPAN- **29**, 325–330 (1995)

22. Milkov, A.V., Dickens, G.R., Claypool, G.E., Lee, Y.J., Borowski, W.S., Torres, M.E., Xu, W., Tomaru, H., TràěĘàďÈàďĘàěĘàďĚŁhu, A.M., Schultheiss, P.: Co-existence of gas hydrate, free gas, and brine within the regional gas hydrate stability zone at hydrate ridge (oregon margin): evidence from prolonged degassing of a pressurized core. Earth and Planetary Science Letters **222**(3-4), 829 – 843 (2004). DOI DOI: 10.1016/j.epsl.2004.03.028. URL http://www.sciencedirect.com/science/article/B6V61-4CF17V5-1/2/c6f567324318c060c977823bb2c1f378

23. Nimblett, J., Ruppel, C.: Permeability evolution during the formation of gas hydratees in marine sediments. Journal of Geophysical Research **108**, B9, 2420 (2003)

24. Peszyńska, M., Lu, Q., Wheeler, M.F.: Multiphysics coupling of codes. In: L.R. Bentley, J.F. Sykes, C.A. Brebbia, W.G. Gray, G.F. Pinder (eds.) Computational Methods in Water Resources, pp. 175–182. A. A. Balkema (2000)

25. Peszynska, M., Showalter, R., Webster, J.: Advection of methane in the hydrate zone: Model, analysis and examples. Mathematical Methods in the Applied Sciences **accepted** (2014). URL http://www.math.oregonstate.edu/ mpesz/documents/publications/PSW.pdf

26. Peszyńska, M., Torres, M., Tréhu, A.: Adaptive modeling of methane hydrates. In: International Conference on Computational Science, ICCS 2010, Procedia Computer Science, available online via www.elsevier.com/locate/procedia and www.sciencdirect.com, vol. 1, pp. 709–717 (2010)

27. Pitzer, K.S.: Activity Coefficients in Electrolyte Solutions. CRC Press ((1991))

28. Platteeuw, J., der Waals, J.V.: Thermodynamic properties of gas hydrates II: Phase equilibria in the system H2S-C3H3-H2O at -3Âř C. Recueil des Travaux Chimiques des Pays-Bas **78**, 126–133 ((1959))

29. Rempel, A.W.: Hydromechanical processes in freezing soils. Vadose Zone Journal **11**(4) (2012). DOI 10.2136/vzj2012.0045. URL http://vzj.geoscienceworld.org/content/11/4/vzj2012.0045.abstract

30. Sloan, E., Koh, C.A.: Clathrate Hydrates of Natural Gases, third edn. CRC Press (2008)

31. Tishchenko, P., Hensen, C., Wallmann, K., Wong, C.S.: Calculation of stability and solubility of methane hydrate in seawater. Chemical Geology **219**, 37–52 (2005). DOI 10.1016/j.chemgeo.2005.02.008|ISSN 0009-2541

32. Torres, M., Wallmann, K., Tréhu, A., Bohrmann, G., Borowski, W., Tomaru, H.: Gas hydrate growth, methane transport, and chloride enrichment at the southern summit of Hydrate Ridge, Cascadia margin off Oregon. Earth and Planetary Science Letters **226**(1-2), 225 – 241 (2004). DOI DOI: 10.1016/j.epsl.2004.07.029

33. Torres, M.E., Kim, J.H., Choi, J., Ryu, B.J., Bahk, J.J., Riedel, M., Collett, T.S., Hong, W., Kastner, M.: Occurrence of high salinity fluids associated with massive near-seafloor gas hydrate deposits. In: Proceedings of the 7th International Conference on Gas Hydrates (ICGH 2011), Edinburgh, Scotland, United Kingdom (2011)

34. Zatsepina, O., Buffett, B.: Phase equilibrium of gas hydrate: Implications for the formation of hydrate in the deep sea floor. GEOPHYSICAL RESEARCH LETTERS **24**(13), 1567–1570 (1997). DOI 10.1029/97GL01599

35. Zatsepina, O., Buffett, B.: Thermodynamic conditions for the stability of gas hydrate in the seafloor. Journal of Geophysical Research-Solid Earth **103(B10)**, 24,127–24,139 (1998). DOI 10.1029/98jb02137

National Energy Technology Laboratory

626 Cochrans Mill Road
P.O. Box 10940
Pittsburgh, PA 15236-0940

3610 Collins Ferry Road
P.O. Box 880
Morgantown, WV 26507-0880

13131 Dairy Ashford, Suite 225
Sugarland, TX 77478

1450 Queen Avenue SW
Albany, OR 97321-2198

2175 University Ave. South
Suite 201
Fairbanks, AK 99709

Visit the NETL website at:
www.netl.doe.gov

Customer Service:
1-800-553-7681